Available online at www.sciencedirect.com

SciVerse ScienceDirect

Ceramics International 39 (2013) 7759–7766

CERAMICS INTERNATIONAL

www.elsevier.com/locate/ceramint

Deposition and characterization of nanocrystalline and amorphous Ni–W coatings with embedded alumina nanoparticles

Saeed Yari, Changiz Dehghanian*

School of Metallurgy and Materials Engineering, College of Engineering, University of Tehran, Tehran, Iran

Received 14 December 2012; received in revised form 2 March 2013; accepted 2 March 2013
Available online 27 March 2013

Abstract

Nanocrystalline and amorphous Ni–W coatings containing Al_2O_3 nanoparticles were electrodeposited from three different ammoniacal citrate baths by direct current (DC) method. The effects of nanoparticles on compositional, structural and morphological features of Ni–W coatings were investigated. The effects of bath chemical composition and current density on codeposition behavior of nanoparticles were also studied. Guglielmi model for particle deposition was applied to identify the kinetics of particle deposition. The presence of nanoparticles may affect on coating grain size, tungsten content and the rate of metal deposition. In addition, nanoparticles can result in more compact coatings with fewer defects. The extent of these effects depends on bath chemical composition and may be influenced by the synergistic effect of Ni on deposition of W. It was also found that the kinetics of particle deposition and the effect of current density on codeposition behavior of nanoparticles are highly dependent on bath chemical composition.

Keywords: B. Nanocomposite; Electrodeposition; Guglielmi model; Ni–W coating

1. Introduction

Ni–W alloy coating has potential corrosion, wear and high temperature resistant properties. Therefore, in recent years, it has been proposed for a variety of applications such as environmentally safe substitute for hard chromium coating or a high temperature coating for bearings, plungers and dies [1–7].

This alloy coating is obtained from citrate baths with or without ammonium ions that contain tungstate and nickel ions. Deposition of this coating occurs through a series of complicated reactions that according to Brenner [8] has been called "induced codeposition". This is due to the fact that tungsten cannot be electrodeposited alone and, in fact, iron group metals such as Ni, Fe and Co can induce the deposition of W and the result will be an alloy. Several mechanisms have been suggested to explain this process. Younes et al. [1,2] proposed that the mixed metal complex of $[(Ni)(HWO_4)(Cit)]^{2-}$ can form in the bath from which the solid solution of tungsten in nickel can be formed, and deposition of nickel can also proceed from its complexes with ammonium or citrate. Podlaha and Landolt [9,10] have studied the induced codeposition of Ni–Mo alloy, which is claimed to have a similar behavior as Ni–W alloy [8]. They believe that the precursor for the deposition of the Ni–Mo alloy is an adsorbed intermediate of the form $[NiCit(MoO_2)]^-_{ads}$ which can be reduced to allow Mo deposition and the reduction of Ni ions follows an independent path. Many other mechanisms have been also suggested that are available in the literature [10,11]. The common facts in all the proposed mechanisms is the synergistic effect of iron-group metals on deposition of W and Mo and that an increase in ammonium and nickel ion concentrations and a decrease in tungstate or molybdate and citrate ion concentrations will boost the rate of alloy deposition.

It is well known that incorporation of micro- or nano-sized carbides and oxides into coatings can enhance their hardness, corrosion, and wear properties [12–20]. This method has been also expanded into Ni–W electrodeposits and in recent years several works have been reported on Ni–W composite coatings with embedded nano- or micro-sized particles. Yao et al. [21] deposited SiC nanoparticles into the Ni–W matrix and an improvement in microhardness, corrosion and wear behavior

*Corresponding author. Tel./fax: +98 21 82084103.
E-mail address: cdehghan@ut.ac.ir (C. Dehghanian).

0272-8842/$ - see front matter © 2013 Elsevier Ltd and Techna Group S.r.l. All rights reserved.
http://dx.doi.org/10.1016/j.ceramint.2013.03.033

of the coating was observed. Boonyongmaneerat et al. [22] claimed that the addition of WC particles to the nanocrystalline Ni–W increases its hardness to a value comparable with that of hard chromium coating. Han and Lu embedded CeO_2 [7] and CeF_3 [23] nanoparticles into the Ni–W coating and have improved high temperature friction behavior and corrosion resistance of the Ni–W coating against molten glass. Hou and Chen [24] have reported that incorporation of Al_2O_3 nanoparticles slightly increased the microhardness of the Ni–W matrix, while the improvement of its tribological properties was remarkable.

The aforementioned studies on Ni–W composite coatings have not illuminated the way by which nanoparticles can affect compositional, structural and morphological features of different Ni–W coatings that have been deposited from different baths. The purpose of this study was to identify these effects, and more importantly, to understand how different bath chemical compositions can kinetically affect the codeposition behavior of nanoparticles with the Ni–W matrix. The most widely accepted model for the kinetics of deposition of inert particles from electrolytic baths has been proposed by Guglielmi [25], whose interpretation is based on a two-step adsorption mechanism. According to the author, the first step is assumed to be substantially physical in character which produces a layer of loosely adsorbed particles on the surface. The second step is electrochemical in character and results in a strong adsorption of the particles that will be gradually submerged by the growing metal.

Knowledge of the kinetics of particle deposition and the mechanism of Ni–W deposition helps in better understanding of compositional, structural and morphological characteristics of the nanocomposite Ni–W coatings. This, in turn, can shed more light on studying the protective properties of nanocomposite Ni–W coatings, which is the subject of our future studies.

2. Materials and methods

Ni–W alloy coatings containing Al_2O_3 nanoparticles were electrodeposited by direct current electrodeposition method. Electrodepositions were done in three baths made of reagent grade materials dissolved in distilled water. The chemical composition of the electrodeposition baths is presented in Table 1. In addition, Al_2O_3 nanoparticles in the concentrations of 0, 1, 2.5, 5 and 10 g/L were added to the baths. Sodium lauryl sulfate (SLS) was added to each bath as a surfactant to reduce the agglomeration of Al_2O_3 nanoparticles and to facilitate the release of hydrogen gas. NaOH was also added to the baths to neutralize citric acid and increase the pH of solutions to 8.

Table 1
Chemical composition of the electrodeposition baths.

Bath	$NiSO_4 \cdot 6H_2O$ (mol/L)	$Na_2WO_4 \cdot 2H_2O$ (mol/L)	$C_6H_8O_7 \cdot H_2O$ (mol/L)	NH_4Cl (mol/L)	SLS (g/L)
Bath 1	0.076	0.2	0.45	0.1	1
Bath 2	0.076	0.2	0.45	0.7	1
Bath 3	0.176	0.1	0.45	0.7	1

The cathode electrodes were steel plates of 20 mm × 20 mm dimensions that were polished with SiC abrasive paper up to 2000 grit, following an ultrasonic cleaning in acetone. The specimens were degreased in hot alkaline solution of 40 g/L NaOH and then activated in an acidic solution of 10% H_2SO_4 just prior to immersion in electrodeposition bath. The specimens were rinsed with distilled water between each preparation step. The anode electrode was pure nickel and the ratio of anode to cathode surface area was kept high enough to prevent any probable polarization of the anode and the resulting ohmic drop between the two electrodes. The applied current density was 40 mA/cm^2 in all experiments. The current densities of 10, 20 and 30 mA/cm^2 were also employed in those experiments that were intended to investigate the effect of current density. The bath temperature was fixed at 60 °C and stirring was done by a magnetic stirrer at a constant speed of 150 rpm. Electrodeposition was done for 1 h.

Surface morphology of the coating was characterized by Mira TESCAN field emission scanning electron microscope. The coating thickness was determined by analyzing the cross-section of the coated plate by Vega TESCAN scanning electron microscope. Coating composition was determined by energy-dispersive X-ray spectroscopy (EDS). The structural analysis of the coatings was performed by X-ray diffraction method (XRD, Philips, X'pert, The Netherlands), by using Cu-K_α radiation and scanning in the $2\theta = 20$–80° range. In addition, the XRD patterns were used to calculate the average grain size of the coatings using the well-known Sherrer formula.

To calculate baths faradic efficiency (FE) the weight of each specimen was measured before and after plating and Eq. (1) was used:

$$FE = W/It\ \Sigma c_i n_i F/BM_i \times 100 \quad (1)$$

where W is the weight of the deposit (g), I is the current passed (A), t is the deposition time (h), c_i is the weight fraction of the element (either nickel or tungsten) in the binary alloy deposit, n_i is the number of electrons transferred in the reduction of 1 mol atoms of that element ($n_i = 2$ for nickel and 6 for tungsten), M_i is the atomic weight of that element (g/mol), F is the Faraday constant (96,485.3 C/mol) and B is a unit conversion factor (3600 C/A h). It was assumed that the nominal weight of embedded nanoparticles does not affect the credibility of the equation.

3. Results and discussion

3.1. General properties of the coatings and their tungsten and Al_2O_3 content

Visual observation of the samples showed that uniform and crack-free coatings were obtained from all electrodeposition baths. Shiny silver, dark gray and ivory colored coatings were the plating results from baths 1, 2 and 3, respectively. The

coatings obtained from all electrodeposition baths were very uniform in thickness; Fig. 1 displays a typical image from cross sectional view of a coating obtained from bath 2. Table 2 presents coatings thickness and faradic efficiency of depositions. Figs. 2 and 3 depict tungsten content of the Ni–W matrix and the weight percentage of Al_2O_3 in the coatings obtained from baths 1, 2 and 3 as a function of Al_2O_3 concentration in the bath, respectively. A detailed discussion on Fig. 3 is presented in Section 3.4.

The values given in Table 2 and Fig. 2 make it easy to discern the synergistic effect of iron-group metals on deposition of W. Large variations in bath chemical composition, by changing the electrodeposition bath from 2 to 3, caused the tungsten content of the coating to just change from 19 to about 14.5 at%. Even though the amount of tungstate ions were decreased dramatically, an increase in the nickel ions assisted the deposition of W. This phenomenon prevented a serious drop in the tungsten content of the coating; i.e. the synergistic effect became more pronounced. Moreover, this fact together with an increase in coating thickness showed that both nickel and tungsten were deposited with higher rates from bath 3. Considering the fact that ammonium ion is a strong complexing agent for nickel, with a change in bath chemical composition from 1 to 2 one expects both a major drop in coating

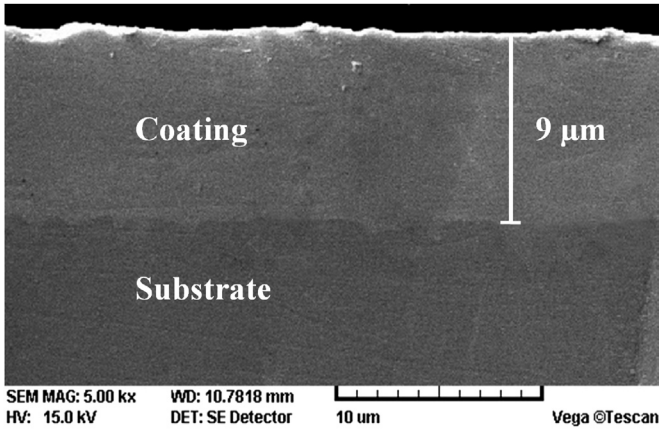

Fig. 1. Cross sectional view of a coating obtained at current density of 40 mA/cm^2 from bath 1 with Al_2O_3 charge of 1 g/L.

Table 2
Coatings thickness and depositions faradic efficiency.

Deposition current density (mA/cm^2)	Bath Al_2O_3 charge (g/L)	Bath 1		Bath 2		Bath 3	
		Coating thickness (µm)	FE (%)	Coating thickness (µm)	FE (%)	Coating thickness (µm)	FE (%)
40	0	8	25.7	9	27.0	22	57.2
40	1	7.5	24	9	26.8	22	57.2
40	2.5	7	22.2	8.5	25.3	22	56.9
40	5	6.5	21.5	8.5	24.7	22	57.3
40	10	6.5	20.6	8	22.6	22	56.9
30	1	5	20.7	5.5	20.9	14	48
20	1	2.5	16.8	3	17.3	8	41.6
10	1	1	14.5	1.5	15.9	3	31.9

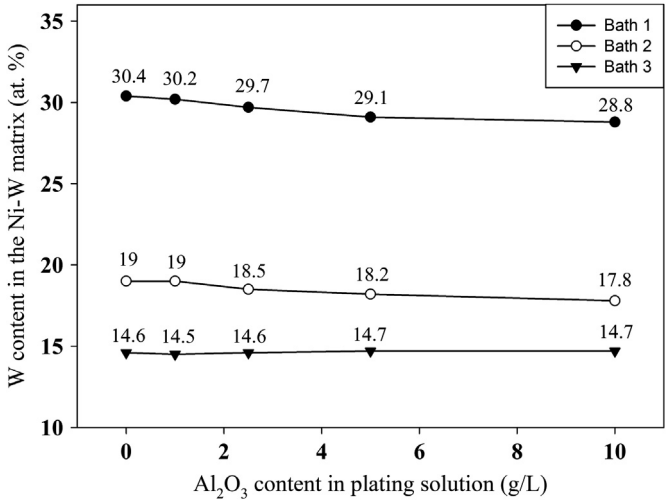

Fig. 2. The effect of nanoparticles on W content of the Ni–W matrix. The numbers show the atomic percent of W.

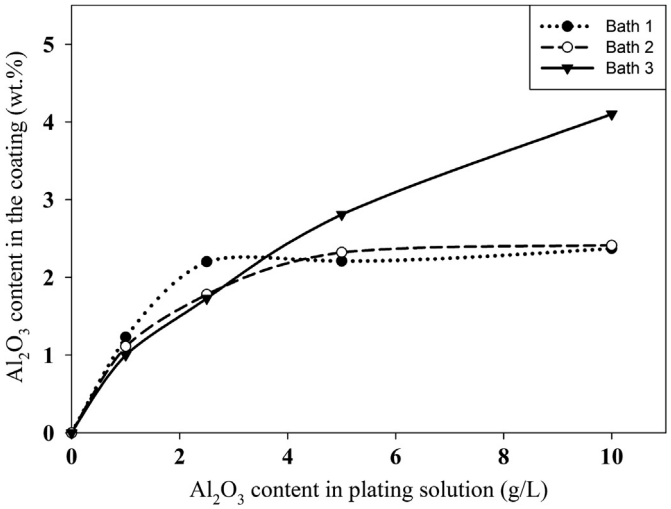

Fig. 3. Al_2O_3 content of the coatings as a function of Al_2O_3 concentration in the electrodeposition bath.

tungsten content and a remarkable increase in bath faradic efficiency and coating thickness. However, the drop in the tungsten content was accompanied by a modest increase in the bath faradic efficiency and coating thickness. This may be due to an increase in hydrogen evolution reaction that restricted metal deposition [26].

It was found that an increase in the amount of nanoparticles in baths 1 and 2 caused a decrease in the bath faradic efficiency and coating thickness. This may be attributed to the presence of nanoparticles which made it difficult for metallic ions to diffuse through the electrolyte and reach the cathode. Correspondingly, it might reduce the rate of metal deposition. This effect was less significant for bath 2, since higher concentrations of ammonium salt means the presence of more complexes of ammonium with nickel ions and as a result, an improvement in ionic diffusion. This prohibitive effect of nanoparticles in electrolytic baths is also reported by other workers [12,13,22]. A decline in ionic diffusion may also cause a decrease in tungsten content of the alloy. According to

Younes et al. [1] and Obradović et al. [26] increasing the electrolyte stirring rate, i.e. improving ionic diffusion, raises the tungsten content of Ni–W electrodeposits. Therefore, a decrease in tungsten content of coatings obtained from baths 1 and 2 may be due to a decline in ionic diffusion. However, these effects were not observed for coatings obtained from bath 3. This may be due to the higher concentrations of depositing ions together with the aforementioned synergistic effect which facilitate the diffusion of ionic complexes that make the deposition of nickel and tungsten possible.

3.2. XRD analysis and coatings grain size

Fig. 4 presents typical XRD patterns for the coatings obtained from baths 1, 2 and 3. The XRD pattern for the coating obtained from bath 1 shows a single broad peak, namely a halo, which is indicative of amorphous nature of the material. On the other hand, the XRD patterns for both coatings obtained from baths 2 and 3 show four peaks. Three of these peaks occurred at 2θ angle of 43°, 51° and 74° which were at slightly lower diffraction angles with respect to the peaks of pure nickel (PDF no. 4–0850). This signifies the formation of solid solution of tungsten in nickel and the peaks can be ascribed to (111), (200) and (220) planes of the FCC-Ni–W, respectively. There is another peak in these patterns at 2θ angle of ~41.4°, where its intensity was dramatically affected by the change in bath chemical composition. It seems it belongs to a highly textured phase, since at least over the whole range of 2θ angles it was occurred alone. This peak does not match with any known phases and it is believed to be for a nonstochiometric tungsten oxide or carbide (because of the presence of carbon from citrate ions in the bath) [4,21,22]. Since the intensity of this peak was negligible for the coating obtained from bath 3, the Ni–W matrix of the coating obtained from this bath can be assumed to be a single-phase structure.

The addition of nanoparticles to the baths did not affect the coatings in terms of phase and their texture and a typical XRD pattern for the coating deposited from either bath is representative of the behavior for the other plated samples obtained from that bath. However, the average grain size of the coatings obtained from XRD patterns indicated that incorporation of nanoparticles caused a decrease in the average grain size of the

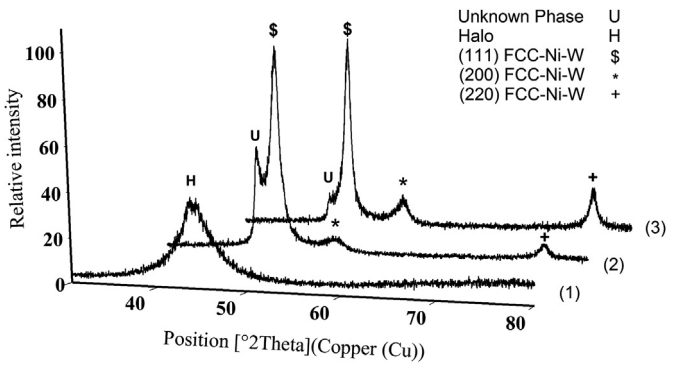

Fig. 4. Typical XRD patterns. Patterns 1, 2 and 3 are for coatings obtained from baths 1, 2 and 3, respectively. Al_2O_3 charge of the baths is 5 g/L and electrodeposition current density is 40 mA/cm^2.

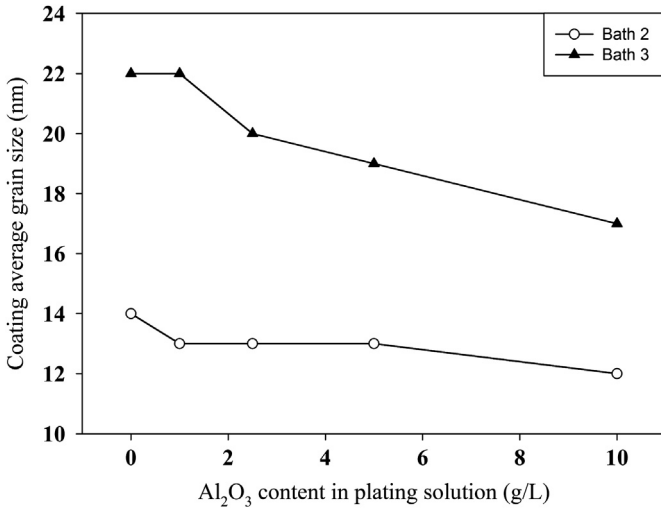

Fig. 5. The effect of nanoparticles on the average grain size of the Ni–W matrix.

coatings obtained from bath 3 (Fig. 5). The embedded nanoparticles can provide more active sites for crystal nucleation and hence restrict the growth of crystallites which in turn causes a decrease in the average grain size [12,13]. This effect was not pronounced for the coatings obtained from bath 2. According to Detor and Schuh [27], the incorporation of tungsten in nickel deposit reduces the coating grain size, therefore the effect of embedded nanoparticles might be compensated by the adverse effect of tungsten degrease in the coating. The absence of Al_2O_3 peaks in the XRD patterns is an indicative of low volume fraction for the embedded nanoparticles.

3.3. FESEM analysis and detection of nanoparticles

Fig. 6 shows the surface morphology of a coating obtained from bath 1 with Al_2O_3 charge of 5 g/L. As it was mentioned, the XRD analysis proved this coating to be amorphous. The cauliflower-like appearance of the coating, which is typical of amorphous materials [28], endorses the XRD analysis. The high amount of tungsten distorted Ni crystals and caused a short-range structural order. The presence of nanoparticles did not affect the surface morphology of the amorphous coating and it was identical to the one without nanoparticles. Similar result was reported for an amorphous Ni–P coating where nanoparticles left the surface morphology of the amorphous coating unchanged [29].

Fig. 7a exhibits the surface morphology of a coating obtained from bath 2 with Al_2O_3 charge of 5 g/L. The same morphology was observed by other workers for the Ni–W coatings free of nanoparticles [6,30]; however at this magnification no detailed information can be obtained. Higher magnification microscopy revealed that the surface had an inhomogeneous morphology (Fig. 7b). The surface consisted of spherical nano-sized grains; meanwhile in some parts a more different morphology with a very strong texture was observed which may belong to an unknown phase that was detected by the XRD analysis. It has been reported that the unknown phase grows on the surface of FCC-Ni–W [31].

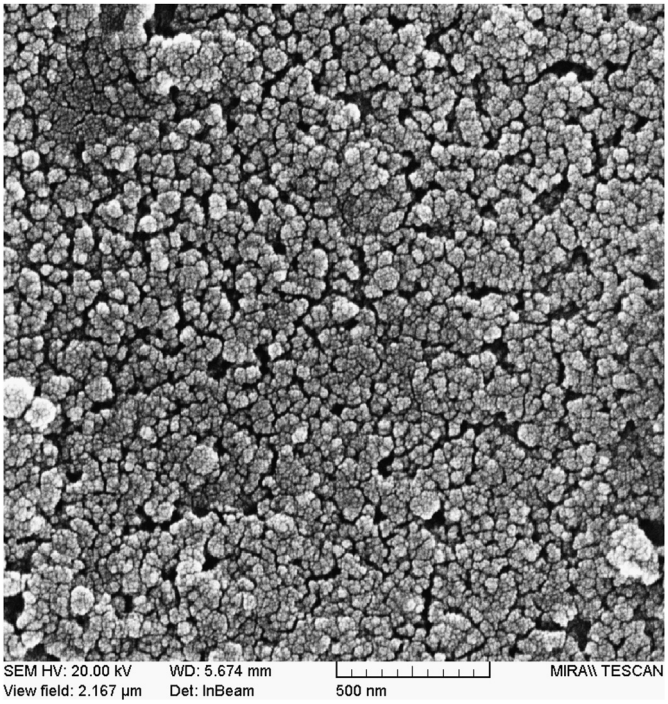

Fig. 6. Surface morphology of the coating obtained at current density of 40 mA/cm^2 from bath 1 with Al_2O_3 charge of 5 g/L.

Because of high level of surface inhomogeneities it was difficult to identify the effect of nanoparticles on surface morphology of the coatings obtained from bath 2. In addition, nanoparticles may not bring any noticeable change to the highly nonuniform surface of these coatings. However, this was not true for the coatings obtained from bath 3, where the addition of nanoparticles modified the surface of these coatings. Fig. 8a and b demonstrates the surface morphology of the coatings obtained from bath 3 with Al_2O_3 charges of 0 and 5 g/L, respectively. It can be seen that a coating with embedded nanoparticles is more compact with fewer defects and microcracks than the one without any nanoparticles. Since, nanoparticles can act as sites for crystal nucleation, their even distribution can lead to a more uniform coating [14,15]. The even distribution of Al_2O_3 nanoparticles was confirmed by elemental mapping of Al, its result is presented in Fig. 9. This figure verifies the presence of Al in the coating and shows that Al_2O_3 nanoparticles were distributed in the Ni–W matrix.

3.4. Kinetics of particle deposition

The weight percentage of Al_2O_3 in the coating as a function of Al_2O_3 concentration in the bath is shown in Fig. 3. For bath 1, addition of nanoparticles up to 2.5 g/L resulted in a relatively sharp increase in the Al_2O_3 content of the coating. However, higher additions of Al_2O_3 nanoparticles to the bath resulted in an almost constant amount of Al_2O_3 in the coating. This was also true for the coatings obtained from bath 2, though the primary increase in Al_2O_3 content of the coating was not as sharp as that of the coatings obtained from bath 1. The above-mentioned relationship for the coatings obtained from bath 3 was linear and the Al_2O_3 content of the coating was raised continuously by an increase in the Al_2O_3 concentration in the bath. Note that the change in the tungsten content of the coatings because of either the presence of nanoparticles in the bath or the change in the current density was lower than that to interfere with a true calculation of Al_2O_3 weight percentage. However, the change in the bath chemical

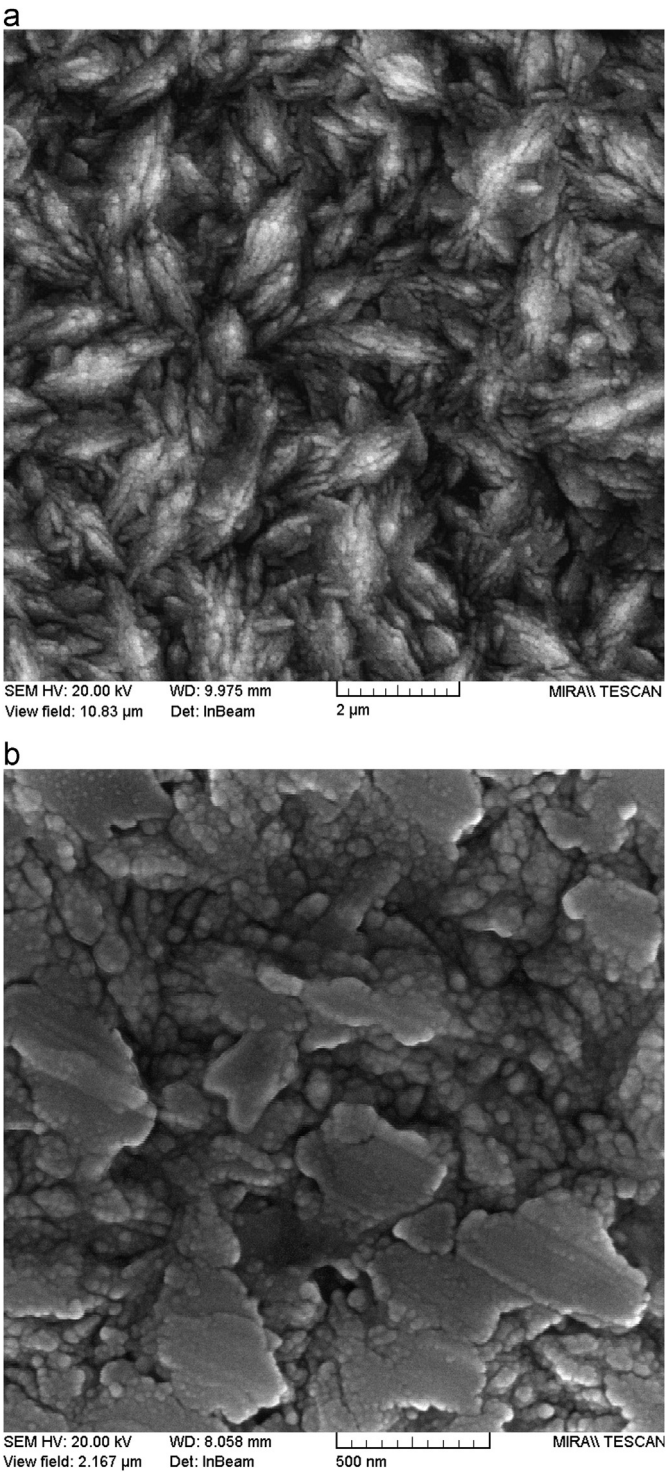

Fig. 7. Surface morphology of the coating obtained at current density of 40 mA/cm^2 from bath 2 with Al_2O_3 charge of 5 g/L at (a) low magnification and (b) high magnification.

Fig. 8. Surface morphology of the coating obtained at current density of 40 mA/cm^2 from bath 3; (a) without nanoparticles and (b) with Al_2O_3 charge of 5 g/L.

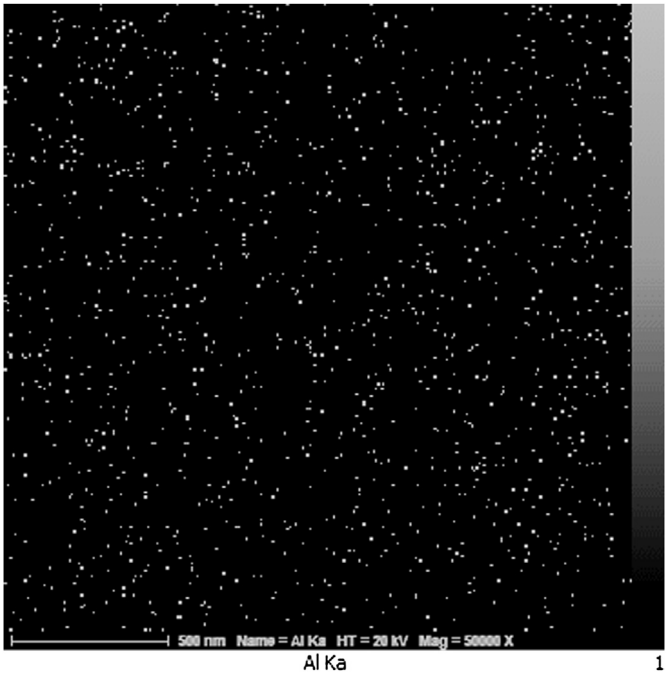

Fig. 9. Elemental mapping of Al for the coating obtained at current density of 40 mA/cm^2 from bath 3 with Al_2O_3 charge of 5 g/L.

composition promoted a dramatic change in the tungsten content of the coatings which makes the calculated percentages of incorporated nanoparticles in the coating obtained from different baths to be incomparable with each other.

The curves in Fig. 3 tend to adopt a linear character by changing the bath chemical composition from 1 to 2 and then to 3. This behavior may be explained by Guglielmi model for particle deposition. According to this model, Eq. (2) shows the relationship between volume fraction of the particles within the deposit, α, and volume percent of the particles in the bath, C:

$$C/\alpha = K\ exp(A–B)\eta(1/k + C) \quad (2)$$

where η is the overpotential for metal deposition. k is the adsorption coefficient and K, A and B are the constants and their values depend on bath chemical composition and the properties of the suspended particles. The constants A and B are of paramount importance; the former is related to the rate of metal deposition and the latter is related to the rate of particle deposition and their relative values determine whether α increases or decreases with η, i.e. the current density.

According to Eq. (2), plotting C/α against C values for each bath gives a straight line. Therefore, one can determine K exp $(A–B)\eta$ (from the slope of the line) and k values (from the intersection of the line with the C axis) for each bath. This has been done for the coatings obtained from baths 1, 2 and 3 (Fig. 10), where d was assumed to be the density of Al_2O_3 nanoparticles. In a constant current density the K exp$(A–B)\eta$ value remains constant, so it is referred as β. To interpret the behaviors displayed in Fig. 3, it is also shown schematically in Fig. 11 that how the changes in β and k values affect the shape of $C–\alpha$ curves; i.e. the curves show volume fraction of the particles in the deposit as a function of volume percent of the particles in the bath.

According to Fig. 10 the β values are 0.107, 0.115 and 0.052 for baths 1, 2 and 3, respectively. The dk values were determined to be 12.92, 8.85 and 1.58 for baths 1, 2 and 3 respectively. The dk values were calculated by extrapolation of the straight lines to the dC axis. Note that k is dimensionless and dk values have the same dimension as d. It can be seen that

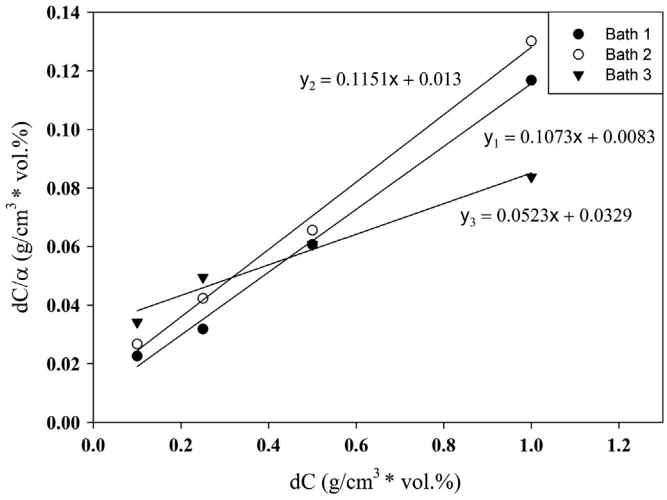

Fig. 10. Codeposition behavior of Al_2O_3 nanoparticles with the Ni–W matrix from different electrodeposition baths according to Eq. (2) (d is the density of nanoparticles).

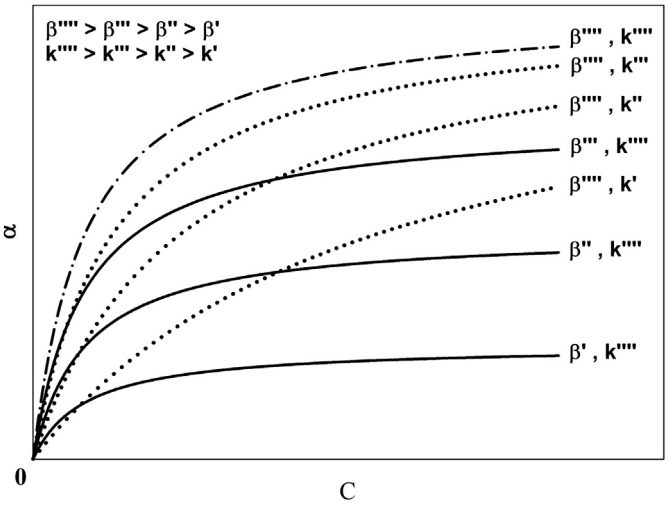

Fig. 11. Schematic representation of the effects of variation of β and k on C–α curve.

β initially increased but then decreased by changing the bath chemical composition from 1 to 2 and then to 3. Neither the irregular change in β values nor the way by which it affects C–α curve (see Fig. 11) suggests that the inclination of the curves in Fig. 3 to linearity stems from the change in β. Meanwhile, the k value decreased as the bath chemical composition changed from 1 to 2 and then to 3. In fact, a coating with a high k value has a high capability to adsorb nanoparticles. Consequently, its surface will be saturated by nanoparticles at lower concentrations of suspended nanoparticles and higher particle loadings will not increase the coating nanoparticle content. Reverse is true for a coating with a low k value and increasing the nanoparticle concentration in the bath will increase the coating particle content and a linear relationship can be observed between the two. This can also be seen in Fig. 11 where the decrease in k value tends to draw the C–α curve to linearity. It may be concluded that the observed variety of relationships between Al_2O_3 concentration in the bath and Al_2O_3 content in the coatings is mainly due to various k values. Therefore, a more linear relationship can be seen between Al_2O_3 concentration in the bath and Al_2O_3 content in the coating for the coating with a lower k value.

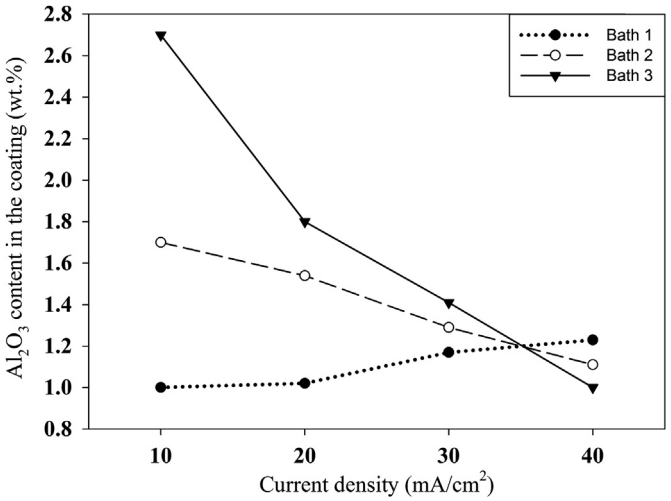

Fig. 12. Effect of electrodeposition current density on Al_2O_3 content of the coating. Al_2O_3 charge of the baths is 1 g/L.

Fig. 12 demonstrates the effect of current density on Al_2O_3 content of the coatings. It was found that an increase in the current density slightly raised the Al_2O_3 content of the coatings obtained from bath 1. According to the Guglielmi model, it seems that for bath 1, the B constant was slightly greater than the A constant. In other words, an increase in current density increased the rate of particle deposition more than that of metal deposition. On the other hand, an increase in the current density reduced the Al_2O_3 content of the coatings obtained from baths 2 and 3, which indicates that the A constant was greater than the B constant for these baths. Therefore, the rate of metal deposition increased more than that of particle deposition. This may be attributed to the higher number of depositing ions in baths 2 and 3, so that a part of them might not interfere with particle deposition. Hence, by more rapid electrodeposition of the metal matrix, fewer nanoparticles were embedded in the coating.

4. Conclusion

Based on the results obtained from this work, following conclusions can be drawn:

1. Three different types of coating were obtained from the baths: an amorphous coating, a nanocrystalline two-phase coating and a nanocrystalline single-phase coating. Addition of nanoparticles does not affect the coatings in terms of phase and their texture.
2. Incorporation of nanoparticles may reduce the coating average grain size, tungsten content and the rate of metal deposition. The extent of these effects depends on bath chemical composition and may be influenced by the synergistic effect of Ni on deposition of W. In addition, the greater the effect of nanoparticles on coating tungsten

content, the smaller will be their effect on coating average grain size.

3. The presence of nanoparticles does not bring a change to the surface morphology of the amorphous Ni–W coating. However, an even distribution of the nanoparticles on the nanocrystalline Ni–W matrix can result in more compact coatings with fewer defects.
4. An increase in the bath Al_2O_3 nanoparticles concentration increases the Al_2O_3 content in the coating, which is more pronounced for a coating with lower capability to adsorb nanoparticles.
5. An increase in electrodeposition current density may increase or decrease the Al_2O_3 content of the coating which depends on bath chemical composition.

References

[1] O. Younes, E. Gileadi, Electroplating of Ni/W alloys, Journal of the Electrochemical Society 149 (2002) C100–C111.

[2] O. Younes-Metzler, L. Zhu, E. Gileadi, The anomalous codeposition of tungsten in the presence of nickel, Electrochimica Acta 48 (2003) 2551–2562.

[3] N. Eliaz, T.M. Sridhar, E. Gileadi, Synthesis and characterization of nickel tungsten alloys by electrodeposition, Electrochimica Acta 50 (2005) 2893–2904.

[4] M.P.Q. Argañaraz, S.B. Ribotta, M.E. Folquer, L.M. Gassa, G. Benítez, M.E. Vela, R.C. Salvarezza, Ni–W coatings electrodeposited on carbon steel: chemical composition, mechanical properties and corrosion resistance, Electrochimica Acta 56 (2011) 5898–5903.

[5] M. Donten, H. Cesiulis, Z. Stojek, Electrodeposition and properties of Ni–W, Fe–W and Fe–Ni–W amorphous alloys. A comparative study, Electrochimica Acta 45 (2000) 3389–3396.

[6] K.-H. Hou, Y.-F. Chang, S.-M. Chang, C.-H. Chang, The heat treatment effect on the structure and mechanical properties of electrodeposited nano grain size Ni–W alloy coatings, Thin Solid Films 518 (2010) 7535–7540.

[7] B. Han, X. Lu, Tribological and anti-corrosion properties of Ni–W–CeO_2 coatings against molten glass, Surface and Coatings Technology 202 (2008) 3251–3256.

[8] A. Brenner, Electrodeposition of Alloys: Principles and Practice, vol. 2, Academic Press, New York, 1963.

[9] E.J. Podlaha, D. Landolt, Induced codeposition: I. An experimental investigation of Ni–Mo alloys, Journal of the Electrochemical Society 143 (1996) 885–892.

[10] E.J. Podlaha, D. Landolt, Induced codeposition: II. A mathematical model describing the electrodeposition of Ni–Mo alloy, Journal of the Electrochemical Society 143 (1996) 893–899.

[11] N. Eliaz, E. Gileadi, Induced codeposition of alloys of tungsten, molybdenum and rhenium with transition metals, in: C. Vayenas, R. E. White, M.E. Gamboa-Aldeco (Eds.), Modern Aspects of Electrochemistry, vol. 42, Springer, New York, 2008, pp. 191–301.

[12] C.T.J. Low, R.G.A. Wills, F.C. Walsh, Electrodeposition of composite coatings containing nanoparticles in a metal deposit, Surface and Coatings Technology 201 (2006) 371–383.

[13] M.R. Vaezi, S.K. Sadrnezhaad, L. Nikzad, Electrodeposition of Ni–SiC nano-composite coatings and evaluation of wear and corrosion resistance and electroplating characteristics, Colloids and Surfaces A: Physicochemical and Engineering Aspects 315 (2008) 176–182.

[14] L. Shi, C.F. Sun, F. Zhou, W.M. Liu, Electrodeposited nickel–cobalt composite coating containing nano-sized Si_3N_4, Materials Science and Engineering: A 397 (2005) 190–194.

[15] L. Mohan, D. Durgalakshmi, M. Geetha, T.S.N. Sankara Narayanan, R. Asokamani, Electrophoretic deposition of nanocomposite (HAp +TiO_2) on titanium alloy for biomedical applications, Ceramics International 38 (2012) 3435–3443.

[16] C. Deyá, B. del Amo, R. Romagnoli, Ceramic microspheres to improve anticorrosive performance of phosphate paints, Ceramics International 38 (2012) 2637–2646.

[17] P. Baghery, M. Farzam, A.B. Mousavi, M. Hosseini, Ni–TiO_2 nanocomposite coating with high resistance to corrosion and wear, Surface and Coatings Technology 204 (2010) 3804–3810.

[18] I. Piwoński, K. Soliwoda, The effect of ceramic nanoparticles on tribological properties of alumina sol–gel thin coatings, Ceramics International 36 (2010) 47–54.

[19] L. Shi, C. Sun, P. Gao, F. Zhou, W. Liu, Mechanical properties and wear and corrosion resistance of electrodeposited Ni–Co/SiC nanocomposite coating, Applied Surface Science 252 (2006) 3591–3599.

[20] A. Eshaghi, R. Mozaffarinia, M. Pakshir, A. Eshaghi, Photocatalytic properties of TiO_2 sol–gel modified nanocomposite films, Ceramics International 37 (2011) 327–331.

[21] Y. Yao, S. Yao, L. Zhang, H. Wang, Electrodeposition and mechanical and corrosion resistance properties of Ni–W/SiC nanocomposite coatings, Materials Letters 61 (2007) 67–70.

[22] Y. Boonyongmaneerat, K. Saengkiettiyut, S. Saenapitak, S. Sangsuk, Effects of WC addition on structure and hardness of electrodeposited Ni–W, Surface and Coatings Technology 203 (2009) 3590–3594.

[23] B. Han, X. Lu, Effect of nano-sized CeF_3 on microstructure, mechanical, high temperature friction and corrosion behavior of Ni–W composite coatings, Surface and Coatings Technology 203 (2009) 3656–3660.

[24] K.-H. Hou, Y.-C. Chen, Preparation and wear resistance of pulse electrodeposited Ni–W/Al_2O_3 composite coatings, Applied Surface Science 257 (2011) 6340–6346.

[25] N. Guglielmi, Kinetics of the deposition of inert particles from electrolytic baths, Journal of the Electrochemical Society 119 (1972) 1009–1012.

[26] M.D. Obradović, R.M. Stevanović, A.R. Despić, Electrochemical deposition of Ni–W alloys from ammonia–citrate electrolyte, Journal of Electroanalytical Chemistry 552 (2003) 185–196.

[27] A.J. Detor, C.A. Schuh, Tailoring and patterning the grain size of nanocrystalline alloys, Acta Materialia 55 (2007) 371–379.

[28] P. Bera, H. Seenivasan, K.S. Rajam, V.K. William Grips, Characterization of amorphous Co–P alloy coatings electrodeposited with pulse current using gluconate bath, Applied Surface Science 258 (2012) 9544–9553.

[29] N. Spyrellis, E.A. Pavlatou, S. Spanou, A. Zoikis-Karathanasis, Nickel and nickel–phosphorous matrix composite electrocoatings, Transactions of Nonferrous Metals Society of China 19 (2009) 800–804.

[30] I. Mizushima, P.T. Tang, M.A.J. Somers, Identification of an anomalous phase in Ni–W electrodeposits, Surface and Coatings Technology 202 (2008) 3341–3345.

[31] R. Juškėnas, I. Valsiūnas, V. Pakštas, A. Selskis, V. Jasulaitienė, V. Karpavičienė, V. Kapočius, XRD, XPS and AFM studies of the unknown phase formed on the surface during electrodeposition of Ni–W alloy, Applied Surface Science 253 (2006) 1435–1442.